Virologica Sinica 40 (2025) 419–429

Contents lists available at ScienceDirect

Virologica Sinica

journal homepage: www.keaipublishing.com/en/journals/virologica-sinica
www.virosin.org

Research Article

Compromised efferocytosis during aging is related to COVID-19 severity in mice

Xianliang Ke [a,b,1], Xian Lin [a,b,c,1], Jin Wang [d], Minqi Chen [e], Xiaoqin Jian [a,b,f], Chang Ye [a,b,f], Quanjiao Chen [a,b,*]

[a] CAS Key Laboratory of Special Pathogens and Biosafety, Wuhan Institute of Virology, Chinese Academy of Sciences, Wuhan, 430207, China
[b] Center for Biosafety Mega-Science, Wuhan Institute of Virology, Chinese Academy of Sciences, Wuhan, 430207, China
[c] Hubei Jiangxia Laboratory, Wuhan, 430207, China
[d] Department of Endocrinology & Metabolism, the Third Affiliated Hospital, Sun Yat-sen University, Guangzhou, 510630, China
[e] Key Laboratory of Stem Cells and Tissue Engineering (Ministry of Education), Zhongshan School of Medicine, Sun Yat-sen University, Guangzhou, 510080, China
[f] University of Chinese Academy of Sciences, Beijing, 430207, China

ARTICLE INFO

Keywords:
SARS-COV-2
COVID-19 severity
Aging
Compromised efferocytosis
Alveolar macrophage
Neutrophil

ABSTRACT

Aging is one of the greatest risk factors for morbidity caused by the coronavirus disease 2019 (COVID-19). In older individuals, a dysregulated immune response to severe acute respiratory syndrome coronavirus 2 (SARS-CoV-2) infection contributes to disease severity; however, the underlying mechanism remains elusive. In this study, we established an aging mouse model of COVID-19, successfully replicating the development of a relatively severe disease in older adults. Further single-cell transcriptome analysis revealed a distinct immune cell landscape in the infected lungs, accompanied by an over-activated inflammatory response, especially in aging mice. Compared to young mice, aging mice showed extensive neutrophil activation, NETosis, and a dramatic decrease in the number of alveolar macrophages (AMs). Moreover, as important executors of efferocytosis, AMs exhibited a low efferocytotic gene signature and downregulation of multiple efferocytosis receptors in aged mice. Further analysis indicated that the efferocytosis of neutrophils, whether undergoing apoptosis or NETosis, was compromised after SARS-CoV-2 infection. Since efferocytosis is a key process in inflammatory resolution, impaired efferocytosis may contribute to hyperinflammation in aging lungs. Our study reveals the characteristics and role of efferocytosis in aging mice after SARS-CoV-2 infection and provides valuable insights for the potential treatment of COVID-19.

INTRODUCTION

The spread of severe acute respiratory syndrome coronavirus 2 (SARS-CoV-2) and its emerging variants has been causing devastating loss of human life since 2019 (Tao et al., 2021). Of the infected population, older adults have experienced more severe symptoms and faced greater challenges during the coronavirus disease 2019 (COVID-19) pandemic. Aging has been recognized as the primary risk factor for morbidity and mortality in the elderly population (Bartleson et al., 2021). Natural aging can result in uncoordinated immune responses that contribute to poor COVID-19 outcomes in older adults, characterized by higher levels of inflammatory cytokines and chemokines, excessive inflammatory cell recruitment into the lungs, delayed virus clearance and inflammation resolution (Bartleson et al., 2021).

Although the age-related immune response directly influences COVID-19 progression, clinical studies of SARS-CoV-2-infected lungs are limited to post-mortem lung samples or bronchoalveolar lavage fluid, which greatly restricts comparative studies of the pathology and immune basis of aging-related vulnerability in COVID-19. This study established an aging mouse model of SARS-CoV-2 infection and compared the immune response in the lungs of young and aged mice using single-cell transcriptome sequencing. To investigate the clues underlying the

* Corresponding author.
E-mail address: chenqj@wh.iov.cn (Q. Chen).
[1] Xianliang Ke and Xian Lin contributed equally to this article.

https://doi.org/10.1016/j.virs.2025.05.008
Received 25 January 2025; Accepted 12 May 2025
Available online 24 May 2025

disease severity in aged mice, the gene expression profiles related to efferocytosis in immune cells of infected mice were systematically analyzed.

RESULTS

SARS-CoV-2 virus causes more severe lung damage in older mice

To elucidate the immune mechanisms underlying the aging-related differences in infection outcomes of SARS-CoV-2, C57BL/6J mice of different ages were infected with mouse-adapted SARS-CoV-2 virus (MAV) (Huang et al., 2021).

Infection with a high dose of 2.25×10^6 pfu MAV resulted in approximately 14.5% weight loss in 19-month-old (19 M) mice at 3 d post-infection (dpi). In contrast, a slight decrease in body weight was observed in infected 3-week-old (3 W) mice (Fig. 1A). Mild damage was observed in the lungs of the 3 W mice, including local signs of inflammatory cell infiltration, fusion of alveolar structures, and edema around the vessels (Fig. 1B). By contrast, necrotizing pneumonia and extensive diffuse alveolar damage were observed around the lungs of 19 M mice, representing excessive neutrophil infiltration and destruction of alveoli in most areas of the lungs (Fig. 1B). Despite the distinct lung pathology in the 3 W and 19 M mice, no significant difference in viral load was observed between the lungs of the two experimental groups (Fig. 1C).

Additional infection experiments were conducted with a broader range of age groups and infection doses to explore the correlation between lung damage and age. Three-week-old (3 W), 3-month-old (3 M), and 13-month-old (13 M) mice were infected with 2×10^4 pfu or 2×10^5 pfu of MAV or mock-infected and observed for a longer period (up to 8 dpi). In all infection dose groups, 3 M and 13 M mice consistently showed greater declines in body weight than the 3 W mice (Fig. 1D and F). The 3 W mice showed no body weight loss after infection with 2×10^4 pfu, or quickly regained weight at 3 dpi after infection with 2×10^5 pfu. The 3 M mice began to regain body weight at 4 dpi; however, at a much lower rate. In contrast, the 13 M mice continued to lose weight until 5 or 7 dpi, showing no signs of body weight recovery until the end of the experiment. Deaths were observed only in the 13 M group. Specifically, 40% (2/5) and 50% (3/6) of the 13 M mice infected with 2×10^4 pfu of SARS-CoV-2 died or reached the humane endpoint (>20% weight loss) after infection. In contrast, all infected mice in the 3 W and 3 M groups survived throughout the experiment (Fig. 1E and G, and Supplementary Fig. S1). No significant difference in viral load was detected among the three infected age groups (Fig. 1H). Histological examination of the lungs revealed age-related differences in tissue damage (Fig. 1I). The results showed a correlation between age and severity of lung damage caused by SARS-CoV-2 infection, similar to observations in humans (Gonzalez et al., 2021).

The lung immune cell atlas alternation post-SARS-CoV-2 infection

To explore the mechanisms underlying severe outcomes in old mice infected with SARS-CoV-2, 3 W and 19 M mice were used for single-cell transcriptome studies. At 3 dpi, lung immune cells from three mice in each group were enriched for single-cell RNA sequencing (scRNA-seq) (Fig. 2A). A total of 35,445 cells passed the cell ranger, and 27,014 high-quality cells, ruling out doublets, were detected in the lungs of the four groups (Fig. 2A, Supplementary Fig. S2).

Based on the expression of cell markers, we identified 23,957 immune cells (3W without infection, 5807; 19 M without infection, 6457; 3W with infection, 6037; 19 M with infection, 5656), including natural killer (NK) (*Gzma*, *Prf1*, *Klra4*, *Nkg7*), T (*Cd3d*, *Cd3g*), and B (*Cd79a*, *Cd79b*, *Igkc*, *Ighm*, *Ebf1*) cells; neutrophils (*S100a8*, *S100a9*, *Stfa2l1*); $CCL3^+$ (*Ccl3*, *Ccl4*, *Ccrl2*, *Gadd45b*), $Ly6c^{high}$ (*C1qa*, *C1qb*, *C3ar1 Ms4a7*), and $Ly6c^{low}$ (*Adgre4*, *S100a4*, *Treml4*) monocytes; $Ki67^+$ macrophages (*Ki67*, *Top2a*, *Stmn1*, *Cenpf*); and alveolar macrophages (AMs) (*Lpl*, *Chil3*, *Plet1*, *Mrc1*, *Atp6v0d2*) using known markers (Fig. 2A–C, Supplementary Fig. S3, S4). The expression profiles of marker genes (Supplementary Fig. S3) and gene clustering analysis (Supplementary Fig. S4) suggest that the isolated cells are predominantly pulmonary immune cells. Compared with mock-infected 3 W mice, 19 M mice without infection showed higher proportions of neutrophils (1.59-fold, 16.9/10.6) and $Ly6c^{high}$ monocytes (2.00-fold, 3.6/1.8), and lower proportions of B cells (0.90-fold, 22.8/25.3), AMs (0.80-fold, 27.5/34.2), and $Ki67^+$ macrophages (0.35-fold, 1.9/5.5) (Fig. 2D), suggesting innate differences in the lung-resident immune cells between the two age groups. After SARS-CoV-2 infection in both 3 W and 19 M mice, B cells, $Ki67^+$ and alveolar macrophages significantly decreased while neutrophils, $CCL3^+$, and $Ly6c^{high}$ monocytes significantly increased.

A higher percentage of neutrophils (20.8/13.1, 1.59-fold) and $Ly6c^{high}$ monocytes (32.7/18.2, 1.80-fold) were observed in aged mice than in young mice, whereas lower proportions of B cells (9.8/17.4, 0.56-fold), $Ki67^+$ macrophages (1/3.8, 0.26-fold), and AMs (6.8/11, 0.62-fold) were detected in aged lungs (Fig. 2D). Moreover, $CCL3^+$ monocytes, which emerged after SARS-CoV-2 infection as an infection-specific cell population, showed a 62.5-fold (12.5/0.2) and 22.0-fold (6.6/0.3) increase in 3 W and 19 M mice, respectively (Fig. 2D). Additionally, compared to the mock-infected groups, a 1.63-fold (5.7/3.5) increase and a 1.32-fold (4.1/3.1) decrease in NK cells were observed in 3 W infection group and 19 M infection groups, respectively, suggesting different NK cell responses in 3 W and 19 M mice following SARS-CoV-2 infection (Fig. 2D). Collectively, the distinct compositions of lung immune cells in 3 W and 19 M mice, both before and after SARS-CoV-2 infection, may underlie their divergent infection outcomes.

SARS-CoV-2 infection activats the inflammatory response in lung immune cells

We next analyzed how the nine previously identified immune cell types contributed to the immune response against SARS-CoV-2 infection (Fig. 3, Supplementary Fig. S3). The results showed that monocytes and macrophages are predominant cell types harboring detectable SARS-CoV-2 RNA (Supplementary Fig. S5). Although only a small proportion tested positive for SARS-CoV-2 RNA-positive, likely due to technique limitations, inflammatory pathways, as indicated by the inflammatory cytokine and chemokine scores, were markedly upregulated in $CCL3^+$ monocytes, $Ly6c^{high}$ monocytes, and AMs (Fig. 3A–C), suggesting that these cells play important roles in eliciting the inflammatory response. High inflammatory cytokine and chemokine scores were observed in $CCL3^+$ monocytes in both mock and infected mice (Fig. 3A–C), but the proportion of $CCL3^+$ monocytes significantly increased after infection (Fig. 2D), implying that $CCL3^+$ monocytes may be an important source of inflammation (Supplementary Fig. S6).

Among the nine cell populations, neutrophils showed the highest inflammatory cytokine and chemokine scores (Supplementary Fig. S6), suggesting that they were highly activated after infection. When analyzing specific gene expression patterns, we observed significantly higher expression levels of interleukin-1 beta (*IL-1B*), C–C motif chemokine ligand 6 (*CCL6*), C-X-C motif chemokine ligand 2 (*CXCL2*), and interferon-induced transmembrane protein 2 (*IFITM2*) in neutrophils from 19-month-old (19 M) mice compared to the 3-week-old (3W) group (Fig. 3D). Conversely, AMs in the 19 M group showed lower expression levels of interleukin 10 receptor subunit alpha (*IL10*RA) and interferon-induced protein with tetratricopeptide repeats 1 (*IFIT1*) following infection than those in the 3W group (Fig. 3E). These findings suggest that although no significant differences were detected in the overall inflammatory and cytokine scores between neutrophils and AMs from 3W to 19 M infected groups, there are substantial differences in their specific inflammatory pathways and functional responses to SARS-CoV-2 infection.

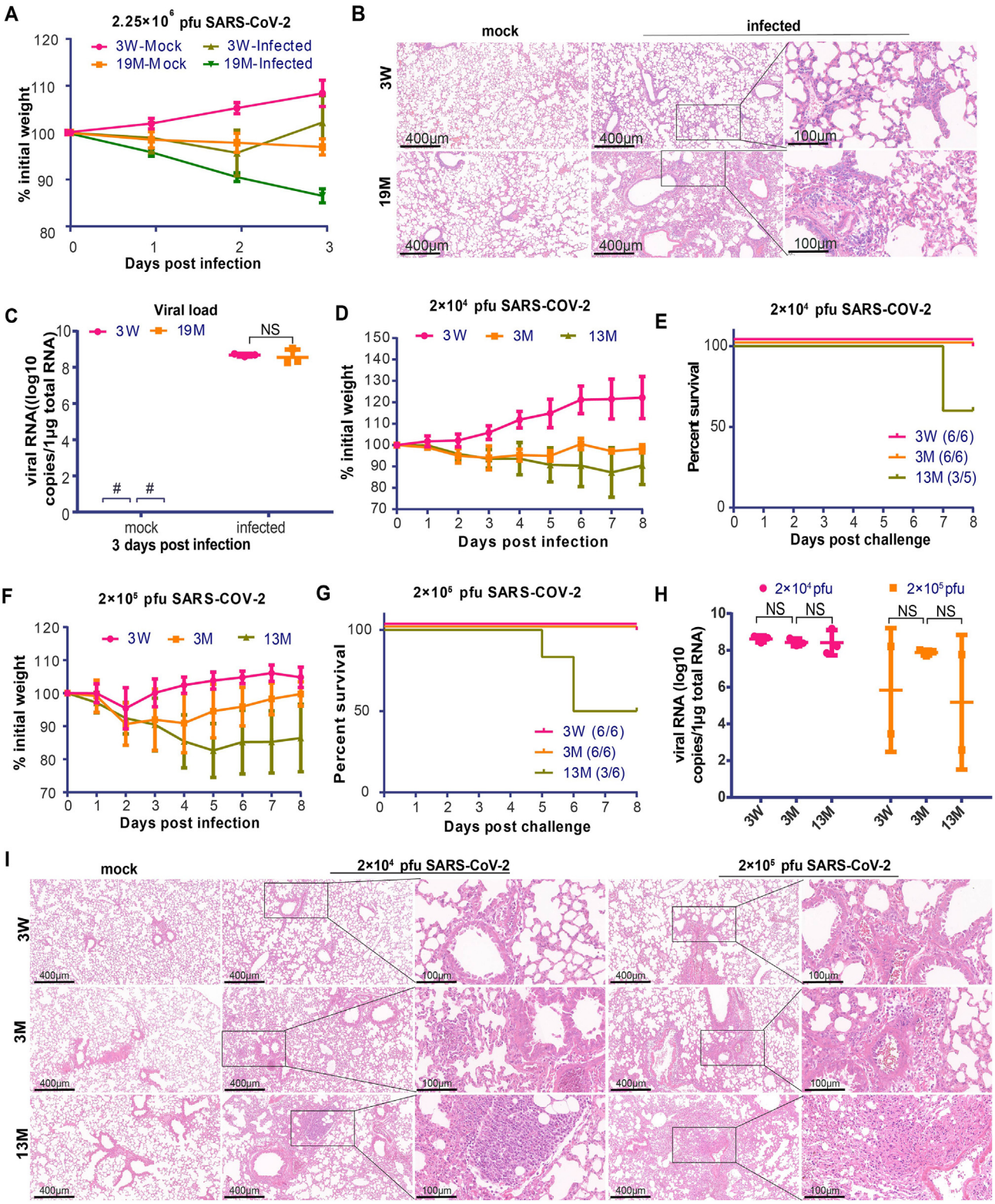

Fig. 1. Comparison of severe acute respiratory syndrome coronavirus 2 (SARS-CoV-2) infection outcomes of mice of different ages. **A–C** Three-week-old (3 W, n = 5) or 19-month-old (19 M, n = 5) mice were intranasally infected with 2.25×10^6 pfu of mouse-adapted SARS-CoV-2 or mock-infected mice, and changes in body weight were monitored daily (**A**). At 3 days post infection (dpi), pathological changes (**B**) and viral load (**C**) in the lungs were detected using real-time PCR (RT-PCR) or hematoxylin and eosin (H&E) staining. Data were shown as mean + SEM. Differences between groups were analyzed using Student's *t*-test. *ns*: not significant. **D–I** 3 W, 3-month- (3 M), and 13-month-old (13 M) mice (n = 5 or 6 for each group) were mock infected or intranasally infected with 2.0×10^4 pfu (**D** and **E**) or 2.0×10^5 pfu (**F** and **G**) SARS-CoV-2 virus, and weight changes and survival rates were recorded until 8 dpi. The viral load and pathological changes in the lungs (n = 3 for each group) were detected at 3 dpi. **I** Pathological changes were detected using hematoxylin and eosin (H&E) staining.

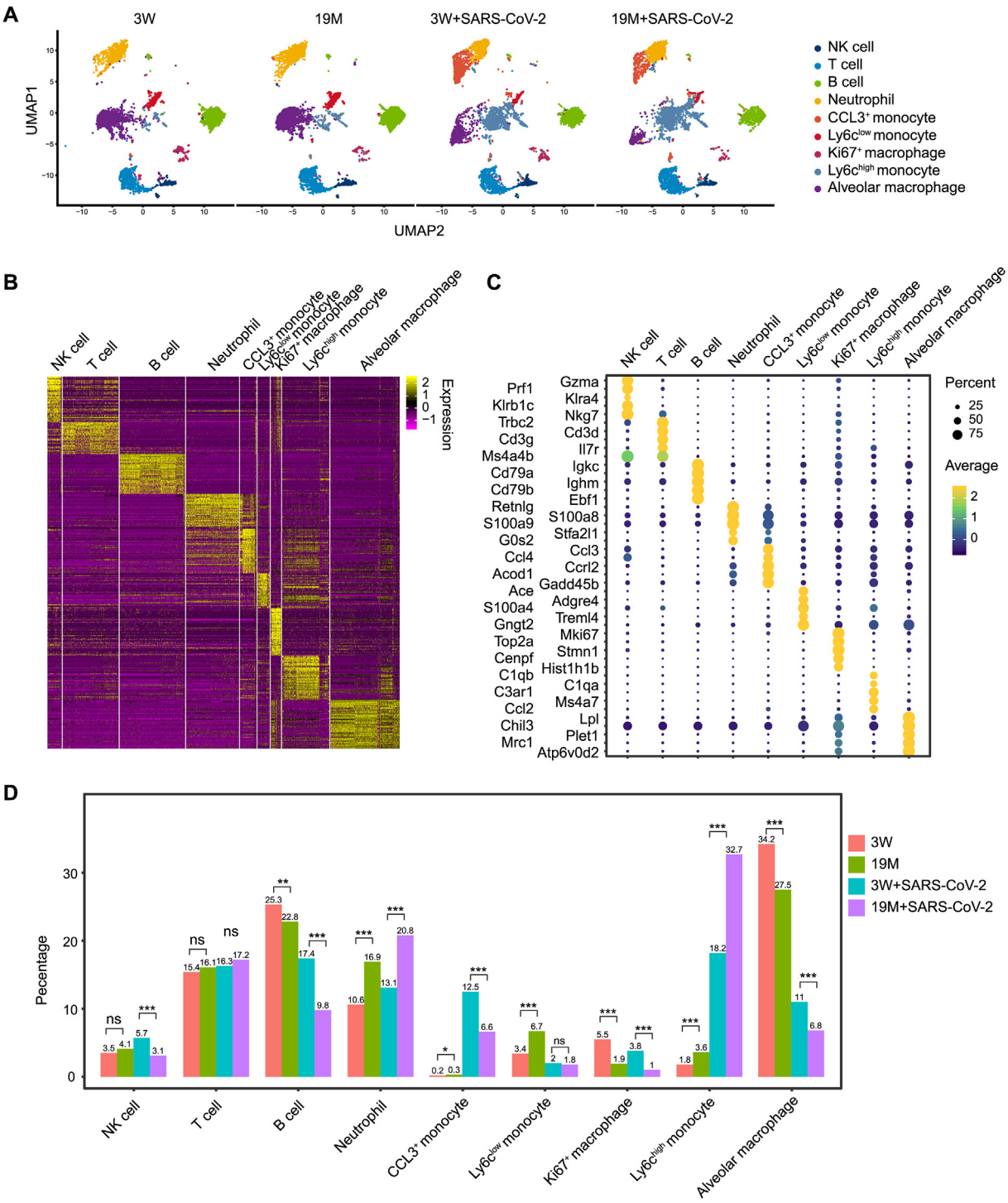

Fig. 2. Lung immune cell atlas during aging upon SARS-CoV-2 infection at the single cell level. **A** Clustering of lung immune cells from 3 W to 19 M mice without or with SARS-CoV-2 infection. **B** Heatmap of signature gene expression in each immune cell type. Columns denote cell types; rows denote genes. Z score, row-scaled expression of the signature genes in each population. **C** Exemplar signature genes from panel **B**. Bubble size indicates the percentage of gene expression, and color indicates the average gene expression. **D** Fraction of each immune cell type from 3 W to 19 M mice without or with SARS-CoV-2 infection. Differences between groups were analyzed using Fisher's test. $*P < 0.05$; $**P < 0.01$; $***P < 0.001$; ns, not significant.

Aged mice exhibited distinct activation of cell death pathways and recruitment of inflammatory cells following SARS-CoV-2 infection

Because immune cell numbers were significantly altered following SARS-CoV-2 infection in both age groups (Fig. 2D), we performed gene ontology (GO) and gene set variation analysis (GSVA) to to assess the enrichment of pathways related to the cell number, including genes involved in cell cycle, proliferation, and death (Fig. 4A, Supplementary Fig. S7 and S8).

Gene expression in AMs, Ki67$^+$ macrophages, and B cells, which showed a significant reduction in cell proportions after SARS-CoV-2 infection, was highly enriched in various cell death pathways (Fig. 4A, Supplementary Fig. S7). Moreover, enrichment of cell death-related

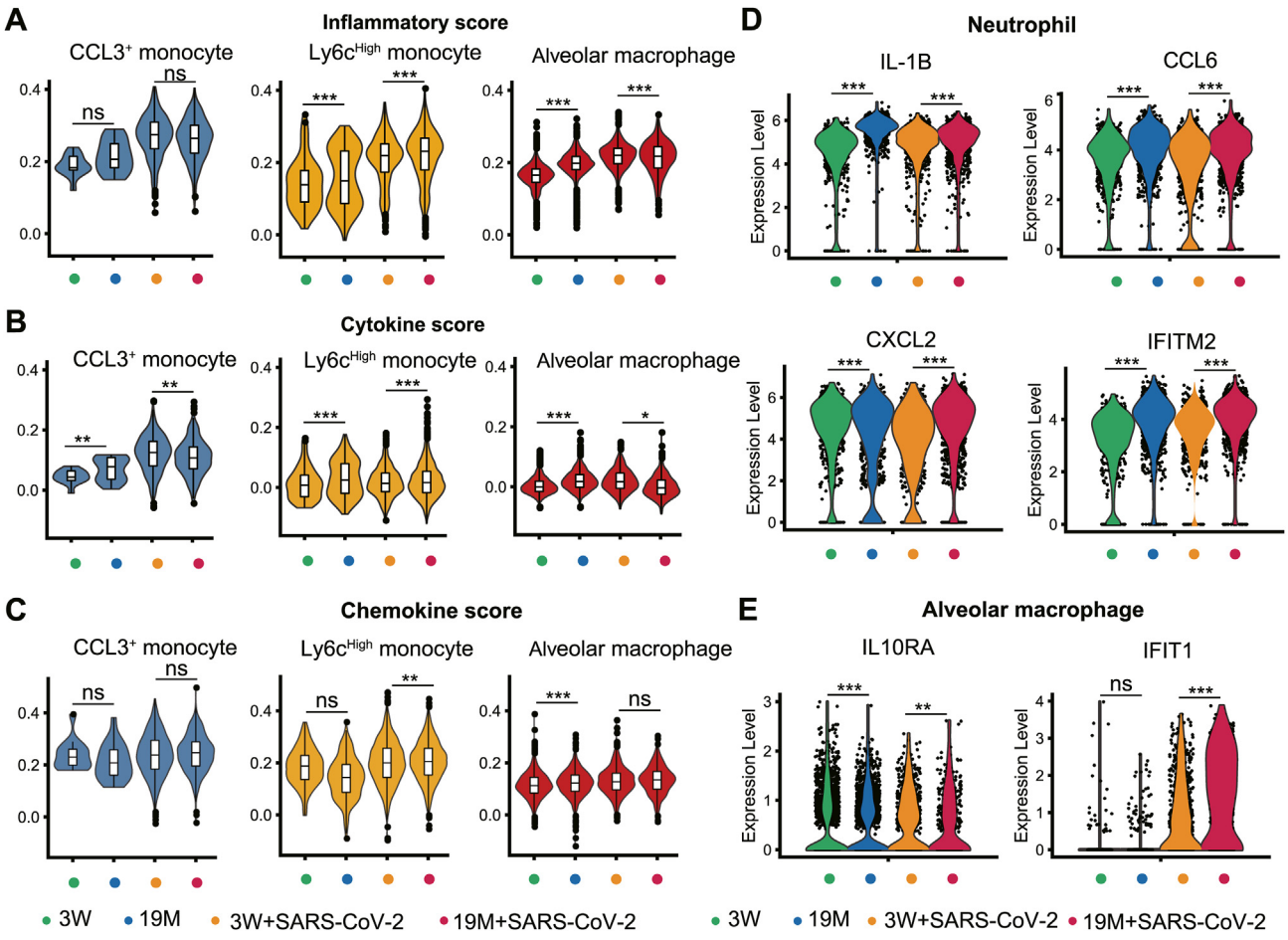

Fig. 3. Analysis of the inflammatory responses and gene expressions in each immune cell type of different groups. **A–C** Inflammatory (**A**), cytokine (**B**), and chemokine scores (**C**) of each immune cell type in 3 W and 19 M mice without or with SARS-CoV-2 infection. Expression of inflammatory, cytokine, or chemokine genes from the GO database in each cell type were analyzed and scores were calculated using the AddModuleScore function of Seurat. **D** Expression of signature genes (*IL-1B*, *CCL6*, *CXCL2*, *IFITM2*) in neutrophils of each group is shown. **E** Expression of *IL10*RA and *IFIT2* in AMs is displayed. Differences between groups were analyzed using Fisher's test. $*P < 0.05$; $**P < 0.01$; $***P < 0.001$; ns, not significant.

genes was also observed in cell types that did not show obvious changes or an increase in proportion after infection (Fig. 2D, Supplementary Fig. S7). The remaining six cell types, including neutrophils (Fig. 4B), NK and T cells, CCL3^{+}, Ly6C^{high}, and Ly6c^{low} monocytes (Supplementary Fig. S7), showed gene enrichment in cell death pathways induced by oxidative stress, ROS, hydroperoxide, and related regulatory pathways in the infected groups.

Neutrophils in the lungs of 19 M mice showed enrichment of pathways regulating cell death induced by oxidative stress, but this was not observed in the lungs of 3 W mice (Fig. 4B). When analyzing the cell death pathways in neutrophils, gene enrichment in the "inflammatory cell apoptotic process", "cell death in response to oxidative stress", and "granzyme-mediated programmed cell death pathways", were found in SARS-CoV-2 infected 19 M mice rather than in 3 W mice, suggesting a different destiny of neutrophils in the two infected groups. After infection, neutrophils either go through the apoptotic pathway or are activated to initiate NETosis, a unique cell death mechanism that usually induces tissue damage (Perez-Figueroa et al., 2021). Genes involved in apoptosis (including *Anxa1*, *Casp4,* and *CD14*) were highly expressed in lung neutrophils from infected 19 M mice; however, these were not expressed in 3 W mice (Fig. 4C), suggesting enhanced apoptosis of neutrophils in the infected 19 M mice.

Additionally, higher expression of genes involved in neutrophil activation processes, such as ROS production (*Cyba*, *Hsp90aa1*, *Rac1*, and *Ncf4*) or expression and secretion of granzymes and granules (*Lcn2*, *Cyba*, *Slc11a1*, *MMP8*, *CD63*, *FPR1*, and *Cr1l*) were found in neutrophils of infected 19 M mice than in the 3 W mice (Fig. 4D), implying that NETosis was also activated in old mice compared to young mice. Indirect immunofluorescence of the lung tissue sections also revealed neutrophil activation, as indicated by the co-localization of histone H3 and myeloperoxidase in the lung (Fig. 4E). Recruited neutrophils, both activated neutrophils that undergo NETosis and those that are not activated and undergo apoptosis, are important contributors to inflammation (Perez-Figueroa et al., 2021). Therefore, excess neutrophils in aging lungs that undergo enhanced NETosis and apoptosis may contribute to the aggregated symptoms in 19 M mice.

This appears to be a paradox between the activated cell death pathways in neutrophils (Fig. 4B) and increased neutrophil numbers (Fig. 2D). We proposed that more neutrophils are recruited upon infection in 19 M mice. To test this hypothesis, we compared the expression of the genes regulating neutrophil recruitment. Neutrophils of 19 M mice were enriched in many more genes involved in chemokine activity, response, and receptor binding than those of 3 W mice (Fig. 4F). Specifically, chemokines (*Ccl2, Ccl5,* and *Ccl7*), which are important for recruiting neutrophils or other inflammatory cells, and chemokine receptors *(Cxcl10, Cxcl16, Ccr5,* and *Cx3cr1*) for neutrophil chemotaxis showed much higher expression levels in infected 19 M mice than in infected 3 W mice (Fig. 4G). This could explain the higher number of neutrophils and Ly6c^{high} monocytes in 19 M mice after SARS-CoV-2 infection than those in the 3 W mice.

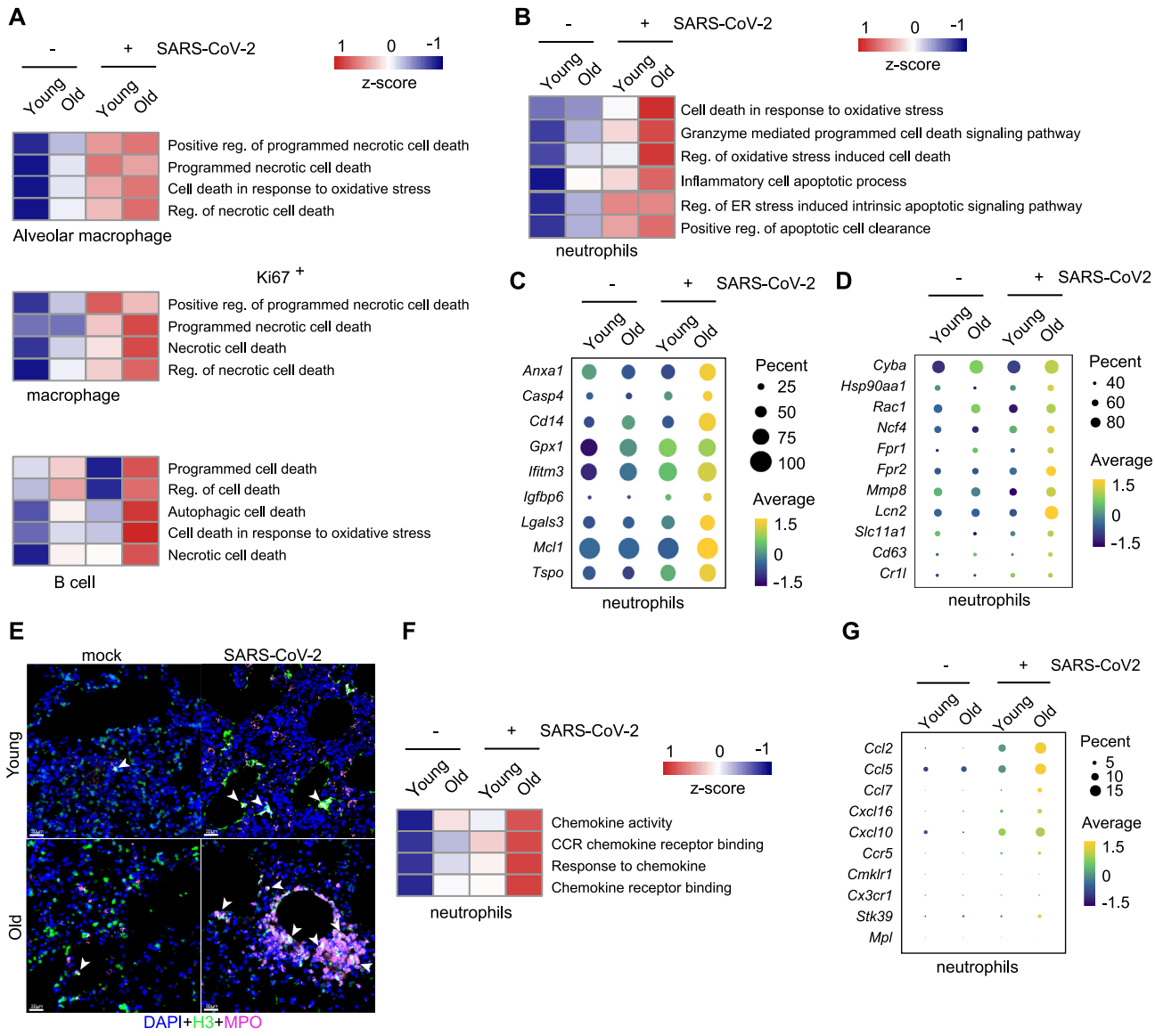

Fig. 4. Analysis of genes involved in cell death and neutrophil recruitment. **A, B** Gene set variation analysis (GSVA) showing the cell death gene pathways in (**A**) macrophages, B cells, and (**B**) neutrophils of 3 W (Young) and 19 M (Old) mice with or without SARS-CoV-2 infection. **C, D** Bubble plot showing apoptosis (**C**) or necrosis (**D**), reactive oxygen species (ROS), and granzyme gene expression in the neutrophils of young and old mice, with or without SARS-CoV-2 infection. **E** Distribution of Histone H3 (green) and Myeloperoxidase (MPO, purple) in the lungs of 3 W and 19 M mice with or without SARS-CoV-2 infection. White arrows indicate $H3^+$ or MPO^+ polymorphonuclear neutrophils. Scale bars, 20 μm. **F** GSVA showing chemokine response pathways in the neutrophils of 3 W and 19 M mice with or without SARS-CoV-2 infection. **G** Bubble plot showing chemokine response genes in the neutrophils of 3 W and 19 M mice with or without SARS-CoV-2 infection. Bubble size indicates the percentage of gene expression, and color indicates the average gene expression (**C, D**, and **G**).

Changes in efferocytosis characteristics of AMs during aging

Activated and apoptotic neutrophils are cleared via efferocytosis to resolve inflammation (Gregoire et al., 2018; Potey et al., 2019). As enhanced NETosis and neutrophil apoptosis were observed in the 19 M infected mice, implying a heavy burden on efferocytes.

A greater reduction in AM numbers, the predominant efferocytes in the lung, was observed after infection, especially in 19 M mice (Fig. 2D). Therefore, we analyzed the gene expression profiles to test whether genes controlling macrophage proliferation were affected by SARS-CoV-2 infection. While AMs of 3 W mice were enriched in genes involved in cell proliferation, such as “positive reg. of cell cycle checkpoint”, “positive reg. of nuclear cell DNA replication” and “positive reg of cell cycle”, AMs in 19 M mice showed poor enrichment in the cell proliferation pathways (Fig. 5A), irrespective of whether they were infected or not. The GO term results were consistent with a lower proportion of AMs in Fig. 2D. Both 19 M and 3 W mice displayed reduced enrichment of cell cycle pathways after infection (Fig. 5A), which may be another important reason for the decrease in AMs caused by SARS-CoV-2, in addition to the improved activation of cell death pathways observed in Fig. 4A.

Subsequently, we analyzed the expression of efferocytosis-related genes to compare the efferocytosis signatures of AMs from the 3 W and 19 M mice. Apoptotic cells express various ligands known as “eat me signals”, which are recognized by receptors on phagocytes directly or indirectly for efferocytosis (Boada-Romero et al., 2020). Therefore, we analyzed and compared the expression of efferocytosis receptors in AMs. A total of 19 efferocytosis receptors in AM were analyzed (Supplementary Fig. S9), of which nine receptor proteins (*Havcr2, Lrp1, Mertk, Axl, Itgb5, Cd36, CD300if, Calr,* and *Cd14*) showed robust expression in mouse AMs (Supplementary Fig. S9), and three of nine (*CALR, P = 0.0016; CD300IF, P = 0.00021;* and *LRP1, P = 1.3E-14*) were expressed at lower levels in 19 M mice than in 3 W mice, either in infected or mock-infected

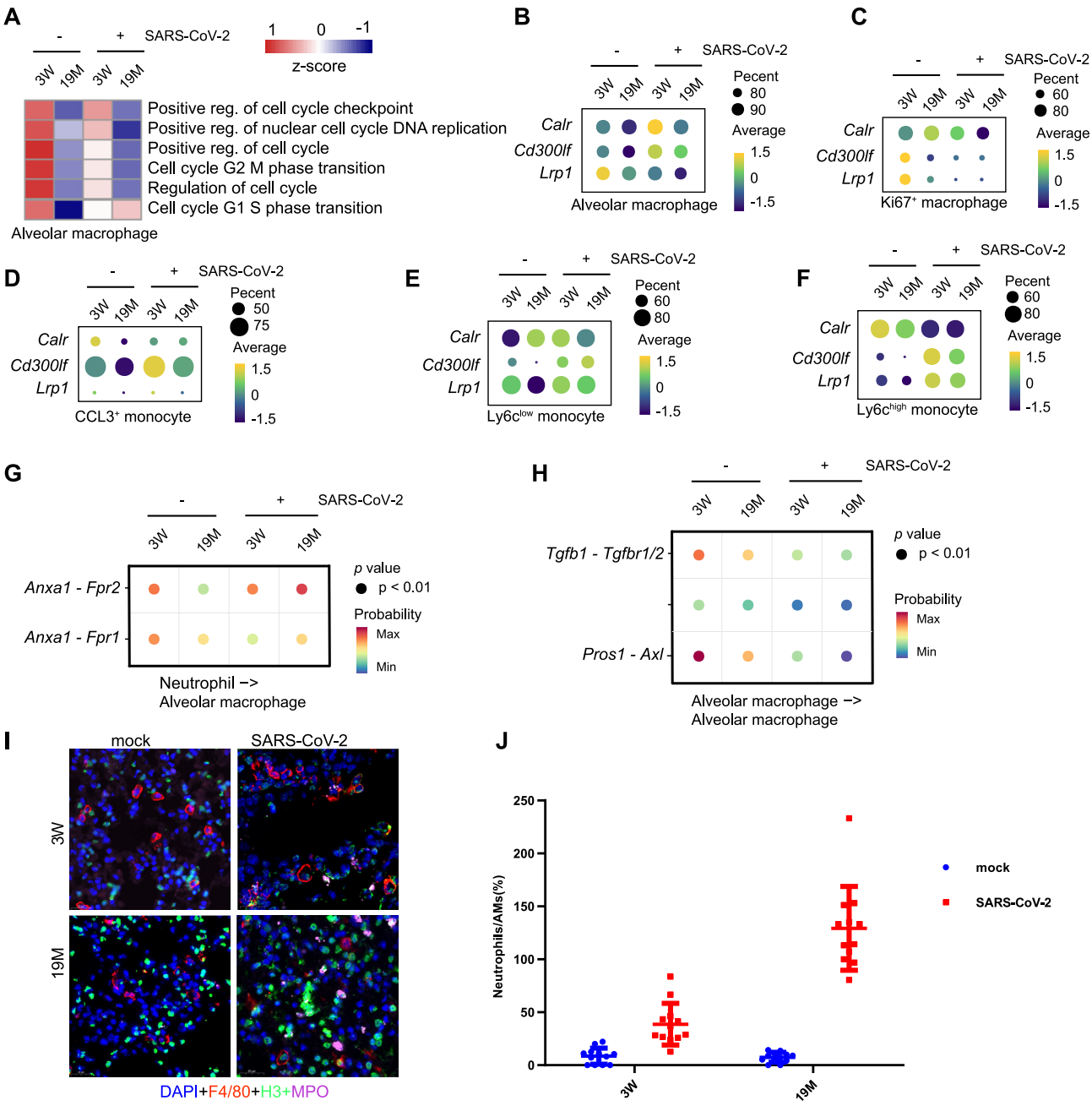

Fig. 5. Efferocytosis signatures of lung immune cells after SARS-CoV-2 infection. **A** Analysis of genes involved in cell proliferation in alveolar macrophages (AMs). **B–F** Bubble plots showing efferocytosis receptor expression in alveolar macrophages (**B**), Ki67^{+} macrophages (**C**), C–C Motif Chemokine Ligand 3+ (CCL3$^{+)}$ monocytes (**D**), Ly6c^{low} monocytes (**E**), and Ly6c^{high} monocytes (**F**). Bubble size indicates the percentage of gene expression, and color indicates the average gene expression. **G–H** Bubble plot of cell communications between alveolar macrophages and neutrophils (**G**), and self-communication of alveolar macrophages (**H**). The colors indicate the mean values of the receptor-ligand pairs between two cell types, and bubble size indicates *P* values. Probability represents the strength or likelihood of communication based on ligand and receptor expression levels. Higher probability indicates stronger potential communication. **I** Lung sections from mice (n = 2 per group) were analyzed across 12 fields (300 μm × 150 μm). Immunofluorescence staining was performed to visualize NETosis and alveolar macrophages (AMs): H3 (green) and MPO (pink) were used to mark NETosis, while F4/80 (red) was used to identify AMs. **J** The efferocytosis activity was quantified by calculating the ratio of MPO-positive punctures (pink) to F4/80-positive areas (red), providing a comparative analysis of efferocytosis characteristics across groups. Scale bars, 20 μm.

groups (Fig. 5B). We also analyzed the expression of these three receptor genes in Ki67^{+} macrophages (Fig. 5C) and monocytes (Fig. 5D–F), which are also important efferocytes. The expression of *CD300IF* and *LRP1* was also lower in CCL3^{+} and Ly6C^{high} monocytes in 19 M mice than in 3 W mice after infection (Fig. 5D and F), indicating changes in efferocytotic receptors with aging. Similarly, *CALR* expression was reduced in Ki67^{+} macrophages (Fig. 5C) and Ly6C^{low} monocytes (Fig. 5E) in 19 M mice compared to 3 W mice following infection, further supporting age-associated alterations in efferocytotic receptor expression.

Furthermore, cell communication networks were analyzed to explore possible changes that influence efferocytosis or inflammation resolution (Supplementary Fig. S10). Multiple cell-cell communication networks involved in M1 polarization, such as MIF, SPP1, and SEMA3, were enhanced in aged AMs (Supplementary Fig. S10). Notably, two important proinflammatory ligands, SEMA3 and MIF, which showed age-related expression patterns, may contribute to the inflammatory status in both mock and infected aging mice (Supplementary Fig. S10). Protein S, an adaptor between phosphatidylserine on antigen-presenting cells and

efferocytosis receptors on AMs, showed weaker interaction with Axl in AMs from 19 M mice than in 3 W mice (Supplementary Fig. S10).

Moreover, the ANXA1-FPR1/FPR2 interaction between neutrophils and AMs, which was previously shown to be an important axis of efferocytosis activation and inflammation resolution, was higher in 3 W mice than in 19 M mice when they were not infected; however, it showed a reversed tendency in infected mice (Fig. 5G). As the number of AMs significantly decreases after infection, the function of ANXA1-FPR1/FPR2 in efferocytosis may not be important, as previously described (Sugimoto et al., 2016). Transforming growth factor beta 1 (TGFB1)-(Tgfbr1+Tfgfbr2), an important mediator of inflammation resolution after efferocytosis (Gregoire et al., 2018), was weaker in infected aged mice (Fig. 5H).

To further validate the efferocytosis capacity of macrophages, we performed immunofluorescence staining on mouse lung tissue sections to detect myeloperoxidase (MPO), histone H3, and F4-80 (a macrophage marker) (Fig. 5I). As MPO is a well-established biomarker for neutrophils in inflammatory conditions, its spatial distribution, along with histone H3, is widely used to assess NETosis activation in mouse lungs. We quantified the ratio of MPO + cells to alveolar macrophages (AMs, marked by F4/80) in the lung sections and observed that this ratio was significantly higher in aged mice compared to the 3-week-old group (Fig. 5J). This finding indicates a potential dysregulation between NETosis clearance and alveolar macrophage function in aged mice. Collectively, these results suggest that the efferocytotic capacity of AMs is compromised in aging mice, which is further exacerbated by the reduced proportion of AMs in the aged lung.

Interactions between neutrophils and other cells reveal the potential role of neutrophils in severe infection outcomes in aged mice

Considering that apoptotic neutrophils or neutrophil extracellular traps (NETs) are less likely to be cleared by efferocytosis in aging mice, we analyzed their possible effects on lung pathology in mice with COVID-19. Comparatively, lung neutrophils in infected aged mice showed high enrichment of genes involved in the absent in melanoma 2 (AIM2) and nucleotide-binding domain, leucine-rich–containing family, pyrin domain–containing-3 (NLRP3) inflammasome complexes, inflammatory responses, and production of molecular mediators of the inflammatory response, cytokine-mediated signaling pathways, and positive regulation of cytokine production (Fig. 6A). Specifically, the *Pycard* gene, an essential part of almost all types of inflammasomes, and important mediators of the NLRP3 inflammasome, including *Casp4*, *Hck*, and *Zbp1*, were enriched in the neutrophils of infected old mice (Fig. 6B). Aging neutrophils also produced higher levels of inflammatory cytokines, including interleukin (*IL)13ra1*, *IL18rap*, *IL1r2*, and *IL1rap* (Fig. 6C), most of which were involved in the IL1/IL18 pathway. Collectively, neutrophils in aging mice probably exert more significant pro-inflammatory effects through the NLRP3-IL1/IL-18 axis.

We also found that chemokines and related genes, such as *Cxcl2, Lgals3, S100A9, Trem1, Trem3,* and *CCL6* (Fig. 6D), were highly enriched in aging neutrophils. Because chemokines play an important role in recruiting inflammatory cells to the lungs after infection, we analyzed the interaction of neutrophils with themselves or with monocytes through chemokines in both 3 W and 19 M mice after infection (Fig. 6E). The interaction between ANXA1-FPR1/FRP2 and CCL6-CCR1, which can recruit monocytes to the infection site (Lafleur et al., 2004; Mcarthur et al., 2015), was enhanced between neutrophils and Ly6C^{high} or Ly6C^{low} monocytes (Fig. 6E). Additionally, the OSM/IL-16 interactions between neutrophils and monocytes or neutrophils, which play important roles in immune cell recruitment after infection (Kerfoot et al., 2001; Hams et al., 2008; Smith et al., 2018; Setiadi et al., 2019), were much stronger in 19 M mice than in 3 W mice (Supplementary Fig. S10). Therefore, neutrophils may also enhance inflammatory responses by recruiting pro-inflammatory cells to the lungs of infected aged mice.

DISCUSSION

In this study, we established an age-related infection model for SARS-CoV-2 infection. Mice with different ages developed age-related pathology that was independent of the viral load, faithfully simulating the dysregulated immunopathology observed in aging individuals.

Compared with young mice, lungs from aging mice were found to recruit more neutrophils with higher apoptotic or NETosis signatures. Neutrophils have been proposed as potential drivers of COVID-19 (Barnes et al., 2020; Hazeldine and Lord, 2021). Products of NETosis contribute to COVID-19 in many aspects; for example, ROS production causes alveolar damage, NETs play a role in immunothrombosis, cytokines contribute to cytokine storms, and chemokines recruit more immune cells (Hazeldine and Lord, 2021). In our study, cell death pathways induced by oxidative stress and ROS were much higher in the immune cells of aging lungs, which may be partially attributed to the excessive number of neutrophils that underwent NETosis (Laforge et al., 2020). We also found an enrichment of genes involved in apoptosis in many immune cells, including neutrophils, in aging mice. These apoptotic cells could release pro-inflammatory chemokines and cytokines. The communication network between neutrophils and other inflammatory cells through chemokine-chemokine receptors further demonstrates the role of neutrophils in the accumulation of inflammatory cells in the lungs. Collectively, features of neutrophils, such as excessive recruitment, high inflammatory scores, pro-inflammatory interactions with other cells, expression profiles of genes involved in neutrophil activation and NETosis, highlighting a critical role of neutrophils in pathogenesis of SARS-CoV-2 in aging mice.

Both apoptotic neutrophils and NETs must be cleared by phagocytes via efferocytosis to quell inflammation and promote tissue repair (Greenlee-Wacker, 2016; Gregoire et al., 2018). However, characteristics of efferocytosis during aging and the relationship between aging efferocytosis and age-associated frailty in response to SARS-CoV-2 have not been studied. By analyzing single-cell transcriptomic data, we revealed several characteristics of aging efferocytosis in the lung: (1) AMs, the major efferocytotic cells, decline during aging, and collapse much more after SARS-CoV-2 infection; (2) aging AMs express lower levels of several efferocytosis receptors, including LRP1, CD300IF, CALR, and ITGB5, which are essential for efferocytosis; (3) several communication networks that modulate AMs reprogramming to efferocytotic-high macrophages (such as SEMA3, MIF, and TGF-b) are impaired in aged AMs. The above factors imply a weaker ability to clear NETs or apoptotic cells in aged mice. Although the relationship between COVID-19 infection and efferocytosis has been widely speculated upon, only a limited number of studies have directly investigated the role of efferocytosis in modulating inflammatory responses following SARS-CoV-2 infection. Furthermore, a small but growing body of research has demonstrated that age-related changes in the expression of efferocytosis mediators, such as TIM-1 or MerTK, play a critical role in clearing invasion microbes such as *Streptococcus* (Bee et al., 2023) or mitigating inflammation caused by cantharidin (De Maeyer et al., 2020). In this context, our study provides a significant, if not unique, contribution to understanding the potential changes in efferocytosis during aging and their implications for COVID-19 outcomes.

The contrast between the surge in pro-inflammatory neutrophils, which needs to be diminished, and the decline in efferocytosis capabilities of AMs, implies an uncontrolled inflammatory state. Therefore, we can infer that impaired efferocytosis could result in the accumulation of ACs and NETosis and continuous recruitment of inflammatory cells, hindering inflammation resolution and tissue repair and delaying the control of viral infection. As a preliminary bioinformatics investigation, this study has inherent limitations that warrant consideration. While the single-cell RNA sequencing data have enabled us to generate compelling hypotheses about the potential role of efferocytosis in SARS-CoV-2 infection outcomes in aged mice, these findings remain to be experimentally validated.

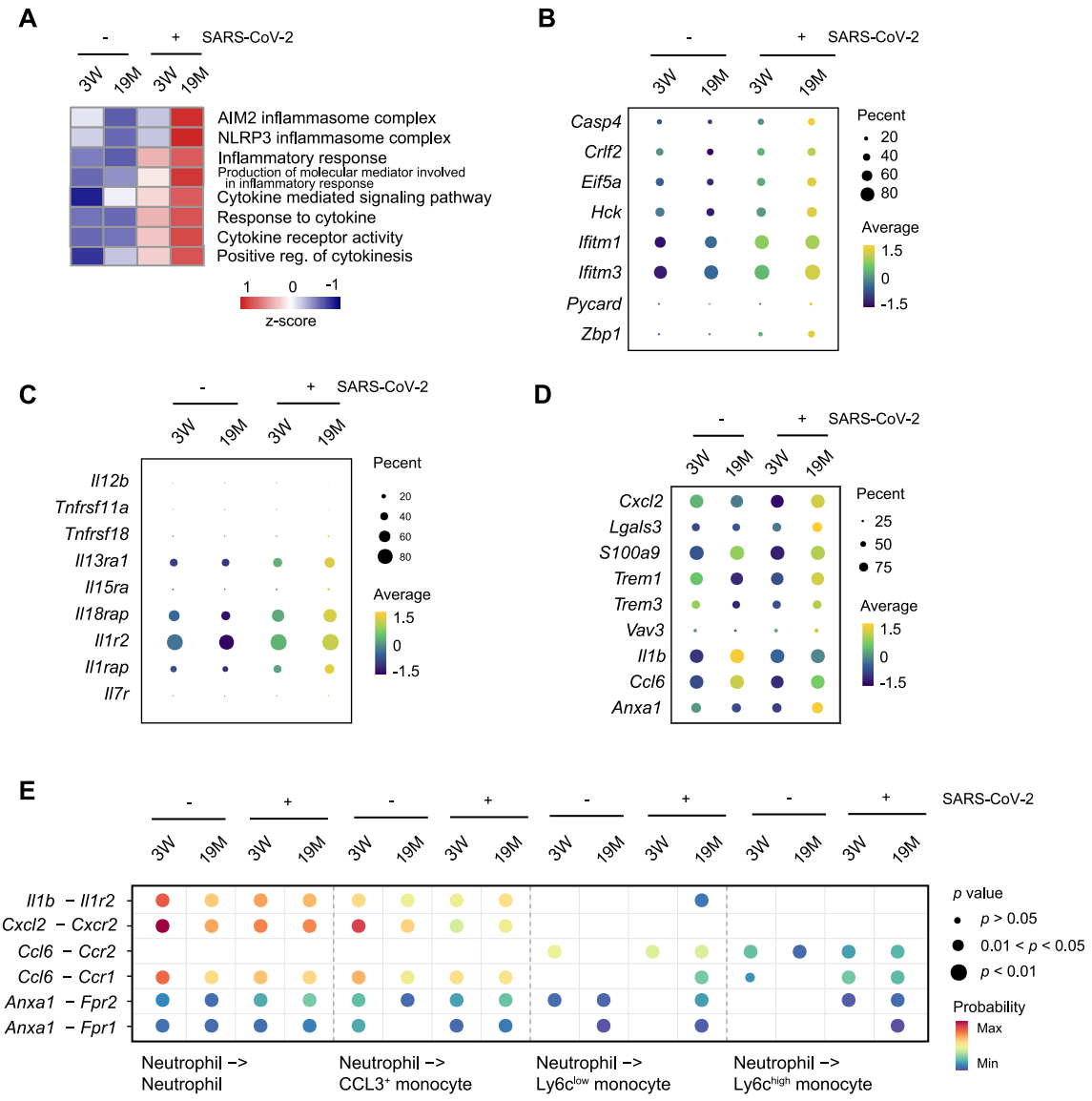

Fig. 6. Proinflammatory genes or cell communication networks in lung neutrophils upon SARS-CoV-2 infection. GSVA (**A**) and bubble plot (**B**) of inflammatory and cytokine response gene expression in neutrophils from 3 W to 19 M mice, with or without SARS-CoV-2 infection. Bubble size indicates the percentage of gene expression, and color indicates the average gene expression. **C–D** Bubble plot of cytokine (**C**) and chemokine (**D**) gene expression in neutrophils from 3 W to 19 M mice, with or without SARS-CoV-2 infection. **E** Bubble plot of cell communication between neutrophils and monocytes in 3 W and 19 M mice, with or without SARS-CoV-2 infection. The colors indicate the means of the receptor-ligand pairs between the two cell types, and the bubble size indicates *P*-values.

CONCLUSIONS

In conclusion, our single-cell transcriptome analysis and histological assessment confirmed the compromised efferocytosis capacity of aging mice and its possible association with the severity of COVID-19. Our findings contribute to the understanding of age-related changes in efferocytosis during SARS-CoV-2 infection and provide clues for harnessing efferocytosis as a potential therapy for COVID-19 in the elderly population.

MATERIALS AND METHODS

Mouse infection

A mouse adapted SARS-CoV-2 virus (MAV) (Huang et al., 2021) was used in this study. C57BL/6J mice were intraperitoneally administered with tribromoethanol (250 mg/kg of body weight) for anesthetization, followed by intranasal infection with MAV diluted in 50 μL Dulbecco's modified Eagle medium (DMEM) (Gibco, USA) for each mouse. For mock-infected control, 50 μL DMEM was intranasally administered for each mouse. All the mice were weighed daily. For the scRNA-seq experiment, mice were sacrificed at 3 dpi, and the lungs were harvested for scRNA-seq preparation, histological analysis, and viral load determination. Mice that lost >20% of their body weight were euthanized and presumed dead in the survival analysis.

Histological analysis

Freshly harvested lungs were fixed with 4% paraformaldehyde, embedded in paraffin, and cut into sections to examine pathogenesis or detect cell markers. For histological analysis, the lung sections were stained with hematoxylin and eosin. Indirect immunofluorescence assays were performed to detect cell markers in lung sections as described previously (Qian et al., 2021). The antibodies and reagents used in this study included an anti-myeloperoxidase antibody (Servicebio, Wuhan, China), anti-Histone H3 antibody (Servicebio, Wuhan, China),

4′,6-diamidino-2-phenylindole (Servicebio, Wuhan, China), anti-LRP1 antibody (Booster Biological Technology, China), and anti-CALR antibody (ProteinTech, Wuhan, China). Slides were scanned using a panoramic MIDI system (3DHISTECH).

Viral load determination

The lungs were homogenized in TRIzol reagent (Invitrogen, USA), and total RNAs were extracted according to the manufacturer's protocol. To quantify the viral loads, 1 μg total RNA was used for real-time polymerase chain reaction (RT-PCR) using the One Step PrimeScript™ RT-PCR Kit (Takara, Japan). The primers and probes have been previously described (Lin et al., 2022). Viral loads were defined as copy numbers of viral RNA in 1 μg total RNA.

scRNA-seq library preparation and sequencing

The whole lungs of three mice from each group were removed, washed in cold phosphate-buffered saline (PBS), and cut into small pieces using scissors. Subsequently, the dissected lungs were washed twice with DMEM and digested with Liberase TM (33.3 μg/mL, Sigma-Aldrich, USA) and DNaseI (133.3 μg/mL, Roche, USA) in 15 mL DMEM at 37 °C for 30 min with rotation. The reaction system was quenched by mixing the reaction system with 30 mL PBS supplemented with 2% fetal bovine serum (FBS). Sequentially, cells were filtered through a 40-μm filter, pelleted by centrifugation at 500×*g* for 8 min, resuspended in 5 mL red blood cell lysis buffer, and incubated at room temperature (~25 °C). After 5 min, the lysis reaction was stopped by adding 10 mL PBS with 2% FBS. Cells were harvested by centrifugation at 500×*g* for 8 min and resuspended in 200 μL PBS with 2% FBS. After filtering through a 35-μm filter, cells were counted under a microscope and diluted to 1×10^6 cells. In total, 12,000 cells were loaded in the lane with 10x Chromium (10x Genomics, USA).

scRNA-seq processing

We aligned scRNA-seq to mm10 reference genome (mm10 reference genomes, 2020), and obtained unique molecular identifier (UMI) counts using Cell Ranger 3.0.2 (Cell Ranger 3.0.2, 2019). Normalization, dimensionality reduction, and clustering were carried out using the Seurat 3.0 R package (Butler et al., 2018). Doublets were eliminated using the default parameters of the DoubletDecon R package. To exclude low-quality cells, cells with >12% mitochondrial content or <200 detected genes were excluded from the Seurat function subset (percentage mt < 15 and nFeature_RNA >200). Preprocessed dataset normalization was performed by dividing the UMI counts per gene by the total UMI counts in the corresponding cells and log-transforming them before scaling and centering. Sctransform normalization was performed with the script: object < - SCTransform (object, vars.to.regress = "percent.mt", verbose = FALSE).

Signature genes of each cluster were obtained using the Seurat function FindMarkers by Wilcox test with fold change >1.5 and *P-value* <0.05 after clustering. Heatmaps, individual Uniform Manifold Approximation and Projection plots, and violin plots were generated using Seurat functions in conjunction with the ggplot2 and heatmap R packages.

Cytokine, inflammation, and chemokine scores were evaluated using the AddModuleScore function of Seurat, using genes from the GO database. Cell-cell communication was conducted using the CellChat R package (Jin et al., 2021), a computational tool designed for systematic analysis of cell-cell signaling networks. The communication probability between cell types was quantitatively assessed based on the co-expression patterns of ligand-receptor pairs, where ligands are expressed in one cell type and their corresponding receptors in another. This probability metric reflects the strength and likelihood of potential cellular interactions, which are computationally derived from the expression levels of interacting ligand-receptor pairs. Communication strength is represented by probability scores, with higher values indicating more robust potential interactions. The analysis distinguishes between two fundamental aspects of cellular signaling: 'incoming' signals, which represent the cellular capacity to receive signals through receptor expression, and 'outgoing' signals, which indicate the cell's potential to send signals via ligand expression. GO analysis was performed using the clusterProfiler R package (Yu et al., 2012) and visualized using the Enrichplot R package (Enrichplot R package, 2020). GSVA was performed using the GSVA R package (Hanzelmann et al., 2013). After log-normalization of expression values, GSVA was performed to calculate the GSVA score of the indicated pathway genes in single-cell datasets with whole protein-encoding genes. Gene sets for GSVA were obtained from the GO database and MSigDB.

Statistical analyses

Data are presented as means ± S.E.M or presented medians, first and third quartiles. The difference was considered statistically significant if $P < 0.05$. For multiple comparisons analysis, data were analyzed by repeated-measures one-way analysis of variance (ANOVA) followed by Dunnett's test. Differences were considered statistically significant if $P < 0.05$. $^*P < 0.05$, $^{**}P < 0.01$, $^{***}P < 0.001$, n.s., not significant. For pairs of measurements, data were analyzed by paired Student's t-test. Differences were considered statistically significant if $P < 0.05$. $^*P < 0.05$, $^{**}P < 0.01$, $^{***}P < 0.001$, n.s., not significant.

DATA AVAILABILITY

The raw and processed scRNA-seq data in this study has been deposited into Gene Expression Omnibus (GEO) database maintained by NCBI (accession number GSM7879994, GSM7879995, GSM7879996, and GSM7879997) and Science Data Bank (https://www.scidb.cn/en) with DOI: 10.57760/sciencedb.23999. Supplementary materials to this article can be found online.

ETHICS STATEMENT

All mouse experiments were performed in National Biosafety Laboratory, Wuhan following the recommendations of the Animal Welfare Committee (ethics number: WIVA04202107).

AUTHOR CONTRIBUTIONS

Xianliang Ke: Conceptualization, investigation, methodology, data curation, formal analysis, writing- original draft, writing-review & editing. Xian Lin: Conceptualization, investigation, data curation, writing-review & editing. Jin Wang: Formal analysis, visualization, writing-original draft, writing-review & editing. Minqi Chen: Formal analysis, methodology. Xiaoqin Jian: Investigation. Chang Ye: Investigation, validation. Quanjiao Chen: Conceptualization, supervision, project administration, writing-review & editing.

CONFLICT OF INTEREST

The authors declare that they have no conflict of interest.

ACKNOWLEDGEMENTS

We thank Prof. Meilin Jin (Huazhong Agricultural University) for kindly providing the mouse-adapted SARS-CoV-2 virus (MAV). We also thank Tao Du and Jin Xiong of National Biosafety Laboratory, Wuhan for their essential support. This work was supported by the National Key Research and Development Program of China (NKPs) (2022YFC2604101). We are grateful for the technical support of the Institutional Center for Shared Technologies and Facilities of Wuhan

Institute of Virology, CAS (Center for Instrumental Analysis and Metrology and Center for Experimental Animals).

APPENDIX A. SUPPLEMENTARY DATA

Supplementary data to this article can be found online at https://doi.org/10.1016/j.virs.2025.05.008.

REFERENCES

Barnes, B.J., Adrover, J.M., Baxter-Stoltzfus, A., Borczuk, A., Cools-Lartigue, J., Crawford, J.M., Dassler-Plenker, J., Guerci, P., Huynh, C., Knight, J.S., Loda, M, Looney, MR, McAllister, F, Rayes, R, Renaud, S, Rousseau, S, Salvatore, S, Schwartz, RE, Spicer, JD, Yost, CC, Weber, A, Zuo, Y, Egeblad, M, 2020. Targeting potential drivers of COVID-19: neutrophil extracellular traps. J. Exp. Med. 217, e20200652.

Bartleson, J.M., Radenkovic, D., Covarrubias, A.J., Furman, D., Winer, D.A., Verdin, E., 2021. SARS-CoV-2, COVID-19 and the ageing immune system. Nat Aging 1, 769–782.

Bee, G.C.W., Lokken-Toyli, K.L., Yeung, S.T., Rodriguez, L., Zangari, T., Anderson, E.E., Ghosh, S., Rothlin, C.V., Brodin, P., Khanna, K.M., Weiser, J.N., 2023. Age-dependent differences in efferocytosis determine the outcome of opsonophagocytic protection from invasive pathogens. Immunity (Camb., Mass.) 56, 1255–1268 e1255.

Boada-Romero, E., Martinez, J., Heckmann, B.L., Green, D.R., 2020. The clearance of dead cells by efferocytosis. Nat. Rev. Mol. Cell Biol. 21, 398–414.

Butler, A., Hoffman, P., Smibert, P., Papalexi, E., Satija, R., 2018. Integrating single-cell transcriptomic data across different conditions, technologies, and species. Nat. Biotechnol. 36, 411–420.

Cell Ranger 3.0.2 https://www.10xgenomics.com/support/software/cell-ranger/downloads. [Accessed 25 January 2024].

De Maeyer, R.P.H., Van De Merwe, R.C., Louie, R., Bracken, O.V., Devine, O.P., Goldstein, D.R., Uddin, M., Akbar, A.N., Gilroy, D.W., 2020. Blocking elevated p38 MAPK restores efferocytosis and inflammatory resolution in the elderly. Nat. Immunol. 21, 615–625.

Enrichplot R package https://github.com/GuangchuangYu/enrichplot. [Accessed 25 January 2024].

Gonzalez, J., Benitez, I.D., Carmona, P., Santisteve, S., Monge, A., Moncusi-Moix, A., Gort-Paniello, C., Pinilla, L., Carratala, A., Zuil, M., Ferrer, R, Ceccato, A, Fernández, L, Motos, A, Riera, J, Menéndez, R, Garcia-Gasulla, D, Peñuelas, O, Bermejo-Martin, JF, Labarca, G, Caballero, J, Torres, G, de Gonzalo-Calvo, D, Torres, A, Barbé, F., CIBERESUCICOVID Project (COV20/00110, ISCIII), 2021. Pulmonary function and radiologic features in survivors of critical COVID-19: a 3-month prospective cohort. Chest (Am. Coll. Chest Physicians) 160, 187–198.

Greenlee-Wacker, M.C., 2016. Clearance of apoptotic neutrophils and resolution of inflammation. Immunol. Rev. 273, 357–370.

Gregoire, M., Uhel, F., Lesouhaitier, M., Gacouin, A., Guirriec, M., Mourcin, F., Dumontet, E., Chalin, A., Samson, M., Berthelot, L.L., Tissot, A., Kerjouan, M., Jouneau, S., Le Tulzo, Y., Tarte, K., Zmijewski, J.W., Tadie, J.M., 2018. Impaired efferocytosis and neutrophil extracellular trap clearance by macrophages in ARDS. Eur. Respir. J. 52, 1702590.

Hams, E., Colmont, C.S., Dioszeghy, V., Hammond, V.J., Fielding, C.A., Williams, A.S., Tanaka, M., Miyajima, A., Taylor, P.R., Topley, N., Jones, S.A., 2008. Oncostatin M receptor-beta signaling limits monocytic cell recruitment in acute inflammation. J. Immunol. 181, 2174–2180.

Hanzelmann, S., Castelo, R., Guinney, J., 2013. GSVA: gene set variation analysis for microarray and RNA-seq data. BMC Bioinf. 14, 7.

Hazeldine, J., Lord, J.M., 2021. Neutrophils and COVID-19: active participants and rational therapeutic targets. Front. Immunol. 12, 680134.

Huang, K., Zhang, Y., Hui, X., Zhao, Y., Gong, W., Wang, T., Zhang, S., Yang, Y., Deng, F., Zhang, Q., Chen, X., Yang, Y., Sun, X., Chen, H., Tao, Y.J., Zou, Z., Jin, M., 2021. Q493K and Q498H substitutions in Spike promote adaptation of SARS-CoV-2 in mice. EBioMedicine 67, 103381.

Jin, S., Guerrero-Juarez, C.F., Zhang, L., Chang, I., Ramos, R., Kuan, C.-H., Myung, P., Plikus, M.V., Nie, Q., 2021. Inference and analysis of cell-cell communication using CellChat. Nat. Commun. 12, 1088.

Kerfoot, S.M., Raharjo, E., Ho, M., Kaur, J., Serirom, S., Mccafferty, D.M., Burns, A.R., Patel, K.D., Kubes, P., 2001. Exclusive neutrophil recruitment with oncostatin M in a human system. Am. J. Pathol. 159, 1531–1539.

Lafleur, A.M., Lukacs, N.W., Kunkel, S.L., Matsukawa, A., 2004. Role of CC chemokine CCL6/C10 as a monocyte chemoattractant in a murine acute peritonitis. Mediat. Inflamm. 13, 349–355.

Laforge, M., Elbim, C., Frere, C., Hemadi, M., Massaad, C., Nuss, P., Benoliel, J.J., Becker, C., 2020. Tissue damage from neutrophil-induced oxidative stress in COVID-19. Nat. Rev. Immunol. 20, 515–516.

Lin, X., Ke, X., Jian, X., Xia, L., Yang, Y., Zhang, T., Xiong, H., Zhao, B., Liu, W., Chen, Q., Tang, C., 2022. Azacytidine targeting SARS-CoV-2 viral RNA as a potential treatment for COVID-19. Sci Bull (Beijing) 67, 1022–1025.

Mcarthur, S., Gobbetti, T., Kusters, D.H., Reutelingsperger, C.P., Flower, R.J., Perretti, M., 2015. Definition of a novel pathway centered on lysophosphatidic acid to recruit monocytes during the resolution phase of tissue inflammation. J. Immunol. 195, 1139–1151.

mm10 reference genomes https://support.10xgenomics.com/single-cell-gene-expression/software/release-notes/build#mm10_2020A. [Accessed 25 January 2024].

Perez-Figueroa, E., Alvarez-Carrasco, P., Ortega, E., Maldonado-Bernal, C., 2021. Neutrophils: many ways to die. Front. Immunol. 12, 631821.

Potey, P.M., Rossi, A.G., Lucas, C.D., Dorward, D.A., 2019. Neutrophils in the initiation and resolution of acute pulmonary inflammation: understanding biological function and therapeutic potential. J. Pathol. 247, 672–685.

Qian, Q., Fan, L., Liu, W., Li, J., Yue, J., Wang, M., Ke, X., Yin, Y., Chen, Q., Jiang, C., 2021. Direct evidence of active SARS-CoV-2 replication in the intestine. Clin. Infect. Dis. 73, 361–366.

Setiadi, H., Yago, T., Liu, Z., Mcever, R.P., 2019. Endothelial signaling by neutrophil-released oncostatin M enhances P-selectin-dependent inflammation and thrombosis. Blood Adv. 3, 168–183.

Smith, S., Wu, P.W., Seo, J.J., Fernando, T., Jin, M., Contreras, J., Montano, E.N., Gabhann, J.N., Cunningham, K., Widaa, A., McCarthy, E.M., Molloy, E.S, Kearns, G, Murphy, CC, Kong, W, Björkbacka, H, Kornfeld, H, Forbess, L, Venuturupalli, S, Ishimori, M, Wallace, D, Weisman, MH, Jefferies, CA., 2018. IL-16/miR-125a axis controls neutrophil recruitment in pristane-induced lung inflammation. JCI Insight 3, e120798.

Sugimoto, M.A., Vago, J.P., Teixeira, M.M., Sousa, L.P., 2016. Annexin A1 and the resolution of inflammation: modulation of neutrophil recruitment, apoptosis, and clearance. J Immunol Res 2016, 8239258.

Tao, K., Tzou, P.L., Nouhin, J., Gupta, R.K., De Oliveira, T., Kosakovsky Pond, S.L., Fera, D., Shafer, R.W., 2021. The biological and clinical significance of emerging SARS-CoV-2 variants. Nat. Rev. Genet. 22, 757–773.

Yu, G., Wang, L.-G., Han, Y., He, Q.-Y., 2012. clusterProfiler: an R Package for comparing biological themes among gene clusters. OMICS A J. Integr. Biol. 16, 284–287.